FEATURE *Technical Application Series by W. Tong*

AN ADAPTIVE BACKWARD IMAGE CORRELATION TECHNIQUE FOR DEFORMATION MAPPING OF A GROWING CRACK IN THIN SHEETS

Large-scale plastic yielding occurs during the fracture process of a ductile thin sheet because plane stress is predominant around an existing notch or crack. Significant plastic deformation can develop before the final rupture of ductile metallic or polymeric materials. Consequently, determination of fatigue and fracture properties of these materials often requires a detailed characterization of the crack-tip deformation field so the energy dissipation via plastic deformation outside the immediate fracture process zone of a crack can be excluded from estimating the essential work of fracture of the material[1–3]. Digital image correlation (DIC) based whole-field deformation mapping tools developed in recent years are ideally suitable for such a task as they have advantages over the traditional moiré laser interferometry in terms of simple sample preparation and low-cost optical set-up[2–7]. However, DIC applications in *complete* crack-tip deformation field measurements currently reported in the literature are still limited partly due to difficulties of analyzing images with newly created irregular sample boundaries (due to the initiation and growth of a crack in the sample). Here a technique is described with an aim to overcome these difficulties in deformation mapping around a growing crack by image correlation. The essential idea of the technique is to combine both *adaptive* grid generation and *backward* image correlation to reliably and efficiently measure the plastic deformation field around a growing crack.

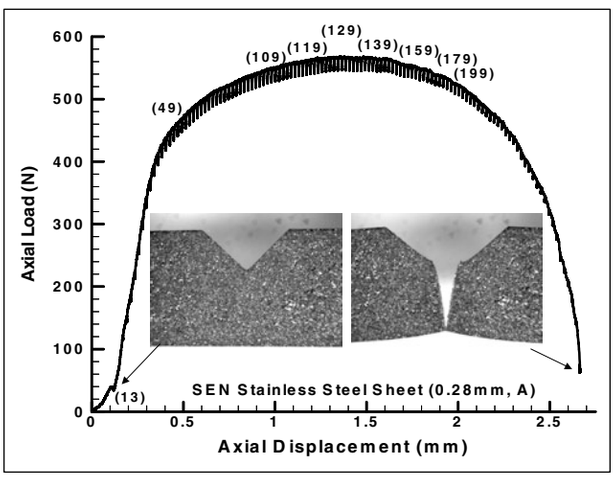

Fig. 1: The load-displacement record of a single-edge notched stainless steel sheet and its fracture under tension (where the tensile loading axis is aligned with the horizontal axis of the images shown). The two images shown are the undeformed and fractured SEN specimen respectively. Initially, the width of the specimen is 9.128 mm and the depth of the V-notch is 3.2 mm.

DEFORMATION MAPPING BY ADAPTIVE BACKWARD IMAGE CORRELATION

Image correlation extracts local deformation variables at a pixel point of a reference image (e.g., a specimen without exerting any loading) by matching the contrast features of a small image region around the pixel point with those of a current image (usually the deformed specimen). Instead of evaluating deformation at every pixel on the reference image, one often analyzes some selected pixels to reduce the computational cost. The selected pixels called a *grid point set* define the image *region of interest* and the small image region around each grid point called a *subset* is used for its local deformation measurement via image correlation. Uniform spacing between the grid points, square or rectangular subsets, and a rectangular region of interest well inside a specimen are almost exclusively used in many DIC deformation mapping applications reported in the literature[2–12]. There are applications such as the tensile loading of a notched specimen shown in Fig. 1 that require the detailed deformation mapping at and near the irregular specimen boundaries. It is proposed that one should define a grid point set adaptively over the irregular specimen shape and their subsets according to the neighboring grid points (see Fig. 2). Similar to a mesh used in a finite element analysis, the density of grid points should be adjusted according to the strain concentration characteristics at notches, cracks, holes, or other cutouts in specimens. The deformation measurement requirements for a high spatial resolution near the high strain gradient region and high accuracy and reliability outside the strain concentration region can thus be effectively balanced.

However, when new specimen boundaries are generated due to crack initiation and growth, an adaptive grid point set defined over an image of the undeformed specimen as the one shown in Fig. 3(a) is not longer valid. One needs to identify the newly created specimen boundaries due to fracture so the discontinuity across the free surfaces of a crack can be excluded from the image correlation analysis to avoid poor correlation and false strain measurements (e.g., see results reported in Refs. 9 and 10). It is rather difficult and impractical to properly define an adaptive grid point set for the cracked specimen over an initial image of the undeformed specimen. It is suggested that one should instead specify the grid point set based on the current image of the cracked specimen and carry out the image correlation analysis in a reversed order (Fig. 3b). Such

Editor's Note: *ET occasionally features short industry/application articles under the title, "Technology Applications." The short articles demonstrate real world application of both measurement techniques and apparatus to be used primarily in industry and, in some cases, the classroom. Please contact Series Editor, Dr. Kristin B. Zimmerman, at kristin.b.zimmerman@gm.com, if you are interested in submitting a Technology Applications article.*

W. Tong is an Associate Professor in the Department of Mechanical Engineering of Yale University, Becton Engineering Center, New Haven, CT.

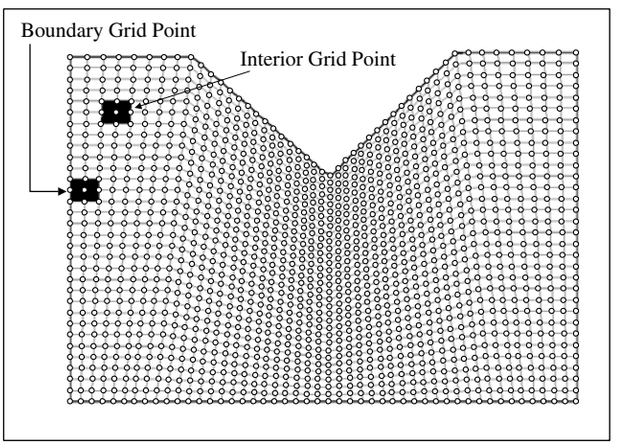

Fig. 2: The schematic of an adaptive grid point set (small open circles) and the associated individual subsets (blackened regions) of boundary and interior grid points used for image correlation. The grid point set is defined over the undeformed specimen (corresponding to image No. 13 shown in Fig. 1).

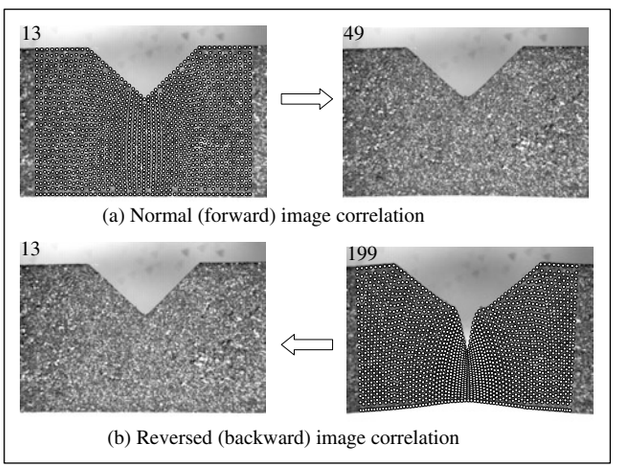

Fig. 3: Schematics of *forward* and *backward* digital image correlation techniques. The grid point set (relatively regular white open circles) is initially defined for the undeformed (reference) image No. 13 in a forward image correlation analysis (a) while the grid point set (adaptive white open circles) is initially defined for the deformed image No. 199 in a backward image correlation analysis (b).

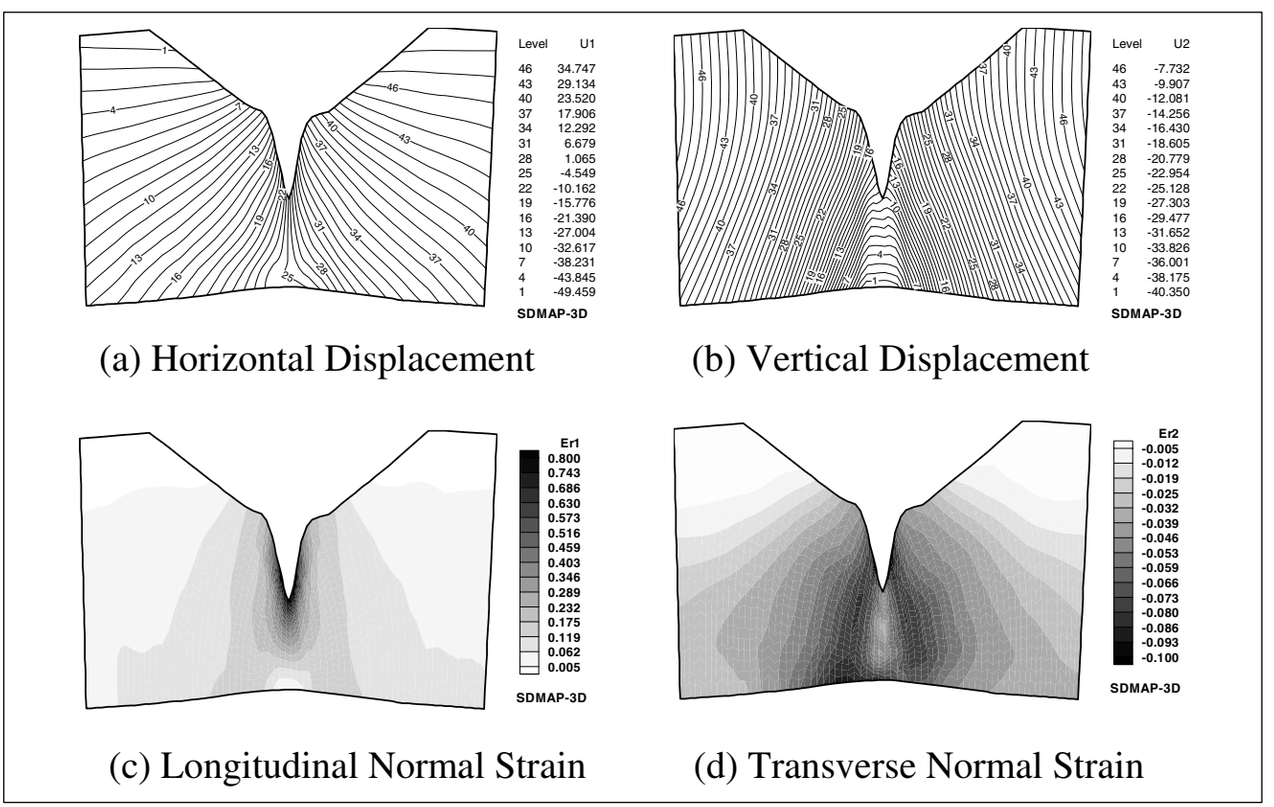

Fig. 4: Selected deformation-mapping results of the cracked stainless steel sheet at an intermediate loading step (corresponding to image No. 199) using the backward image correlation with an adaptive grid point set shown in Fig. 3(b). Each contour line shown in (a) and (b) corresponds respectively to 45 μm and 17 μm horizontal and vertical displacements.

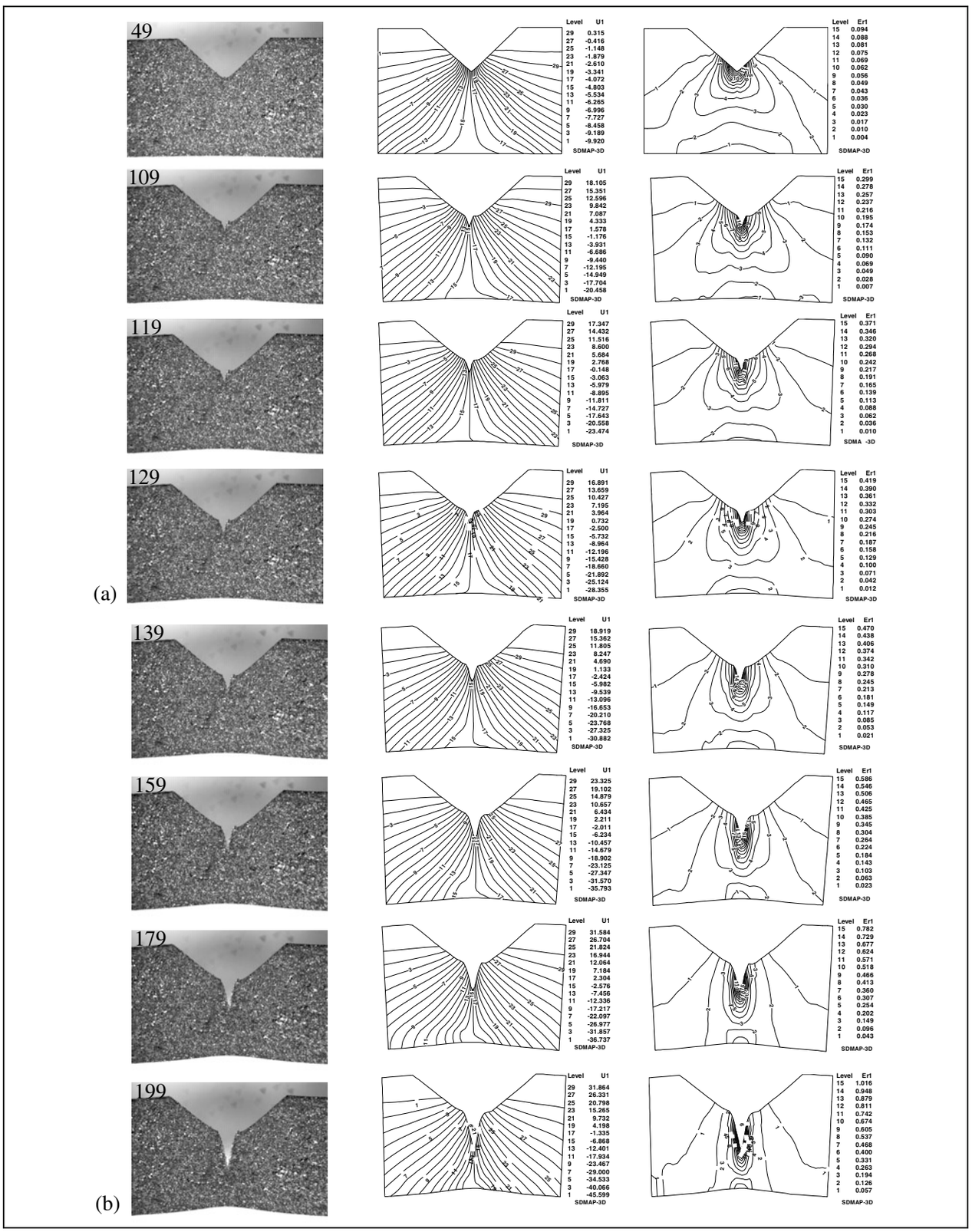

Fig. 5: Evolution of crack initiation and growth in notched stainless steel sheet at eight different load levels (as indicated by the numbered images, see Fig. 1).

an approach has the advantages that allow one to easily identify the specimen boundaries and adaptively adjust grid point density (based on the current deformed shape of the specimen). One needs only a simple post-processing procedure to obtain the usual Lagrangian displacements and displacement gradients from the backward image correlation analysis (see Appendix for details).

AN ILLUSTRATIVE EXAMPLE

The proposed backward digital image correlation technique with an adaptive grid point set is demonstrated in this section by analyzing the digital images acquired during tensile testing of a single edge notched stainless steel sheet.

A rectangular strip of the stainless steel sheet with dimensions of 50 mm long, 9.13 mm wide, and 0.28 mm thick was clamped down at both ends and stretched quasi-statically under displacement control by a compact desktop tensile tester (100 mm-by-125 mm-by-50 mm in total dimensions, a total crosshead travel of 50 mm, and a load cell of 4,400 N maximum capacity). A 90° V-notch with a depth of 3.2 mm was made at one of the edges of the rectangular stainless steel strip and one of its flat surfaces was sprayed with fine black-and-white paint speckles to aid the image correlation analysis. A crack initiated during testing at the tip region of the V-notch and grew along the width direction of the strip gradually. The tensile test was paused frequently so digital images (640-by-480 pixels, 8-bit grayscale) of the stainless steel strip were acquired. The imaging system used includes a telecentric lens (55 mm, Edmund Scientific Inc.), a monochromic CCD video camera, and a frame grabber board. Each digital image was acquired by averaging a total of 60 video frames to minimize noise[5] and more than 200 digital images were recorded for the test. The axial load versus displacement curve of the test is shown in Fig. 1 along with video images of the initially notched and later cracked strip. Multiple small load drops shown on the curve correspond to the times when the test was paused and digital images were acquired. Nine selected images (their numbers in parentheses are placed on the load-displacement curve to indicate the load levels when the images were taken) were analyzed by the newly proposed adaptive backward digital image correlation technique. For images with severe deformation levels or significant image contrast variations, an incremental image correlation procedure[11,12] was also utilized.

The displacement and strain contour plots at the load step of image No.199 are shown in Fig. 4. The grid point set shown in Fig. 3(b) was used in the image correlation analysis to obtain the deformation mapping results between image No. 13 and No. 199. The units for the displacement contour levels are in pixels (1 pixel = 24 μm here) so each contour line corresponds respectively to 45 μm and 17 μm horizontal and vertical displacements. The normal strain distributions around the grown crack at image No. 199 show high concentrations around and ahead of the crack. The evolution of the notch deformation and crack initiation and growth is illustrated via Fig. 5 for a total of eight different load steps. Both horizontal displacement and longitudinal normal strain contour plots show similar patterns with increasing concentrated deformation around the moving crack tip. The crack initiated and grew before the axial load reached its maximum level (see Fig. 1) and the maximum axial true strain level at the crack tip increased monotonically from 9.4% just prior to crack initiation (image No. 49) to more than 100% at the load step of image No. 199. The image pair of No. 13 and No. 49 was also analyzed by forward image correlation using the grid point set shown in Fig. 3(a) as no crack initiation was visually detectable. As expected, little difference was observed in the results by either a forward or a backward correlation analysis for the image pair No. 13 and No. 49.

CONCLUSIONS

An adaptive, backward, and incremental digital image correlation technique is proposed to extract detailed deformation maps around a growing crack in a ductile thin sheet. Experimental results show that such a technique is very robust and effective in deformation mapping measurements of a cracked stainless steel specimen with irregular and newly generated boundaries. Besides one can obtain accurately the crack-tip opening displacement (CTOD) and crack-tip opening angle (CTOA) data for the material being tested. The whole-field deformation measurement results are also readily available to aid and validate finite element fracture analyses. The proposed technique can also be used to improve the spatial resolution and accuracy of mapping nonhomogenous deformation fields inside a diffuse neck of a thin sheet, around interfaces (including interfacial fracture), and in multiphase materials. A possible further development of the proposed technique is to *automatically* detect the current specimen boundaries at each load step using some conventional digital image processing techniques so adaptive grid generation on the current image can be speedily carried out.

ACKNOWLEDGMENTS

The experiment on the crack initiation and growth in a V-notched stainless steel sheet reported here was conducted by Ms. H. Tao at Yale University.

References

1. Ma, L., Kobayashi, A.S., Atluri, S.N., and Pan, P.W., "Crack Linkup: An Experimental Analysis," EXPERIMENTAL MECHANICS, **42** (2), p. 147–152 (2002).

2. Han, G., Sutton, M.A., and Chao, Y.J., "A Study of Stationary Crack-tip Deformation Fields in Thin Sheets by Computer Vision," EXPERIMENTAL MECHANICS, **34** (2), 125–140 (1994).

3. Dawicke, D.S., and Sutton, M.A., "CTOA and Crack-tunneling Measurements in Thin Sheet 2024-T3 Aluminum Alloy," EXPERIMENTAL MECHANICS, **34** (4), 357–368 (1994).

4. Vendroux, G., and Knuass, W.G., "Submicron Deformation Field Measurements II: Improved Digital Image Correlation," EXPERIMENTAL MECHANICS, **38**, p. 86–92 (1998).

5. Smith, B.W., Li, X., and Tong, W., "Error Assessment of Strain Mapping by Digital Image Correlation," EXPERIMENTAL TECHNIQUES, **22** (4), p. 19 (1998).

6. Tong, W., and Li, X., "Evaluation of Two Plastic Strain-mapping Methods, *Proc. of the SEM Annual Conf. on Theoretical, Experimental and Computational Mechanics,* p. 23–26 (Cincinnati, OH, June 1999).

7. Li, X., *Spatial Characterization of Unstable Plastic Flow Patterns in Two Aluminum Alloy Sheet Metals,* Ph.D. Thesis, Yale University, New Haven, CT (2001).

8. Chen, D.J., Chiang, F.P., Tan, Y.S, and Don, H.S., "Digital Speckle Displacement Measurement Using a Complex Spectrum Method," *Appl. Optics,* **32** (1), 1839–1849 (1993).

9. Choi, S., and Shah, S.P., "Measurement of Deformation on Concrete Subjected to Compression Using Image Correlation," *EXPERIMENTAL MECHANICS*, **37** (3), 307–313 (1997).

10. Gonzalez, J., and Knauss, W.G., "Strain Inhomogeneity and Discontinuous Crack Growth in a Particulate Composite," *J. Mech. Phys. Solids,* **46** (10), p. 1981–1995 (1998).

11. Tong, W., "Detection of Plastic Deformation Patterns in a Binary Aluminum Alloy," EXPERIMENTAL MECHANICS **37** (4), p. 452–459 (1997).

12. Tong, W., "Strain Characterization of Propagative Deformation Bands," *J. Mech. Phys. Solids* **46** (10), p. 2087–2102 (1998). ■

APPENDIX

In a planar deformation analysis of a solid, one usually considers the motion of a continuum material point designated by its Lagrangian or material coordinates (X, Y) in a reference configuration as

$$x = X + U(X, Y), \; \mathrm{y} = \mathrm{Y} + V(X, Y), \tag{A1}$$

where (x, y) are the Eulerian or spatial coordinates of the material point in the current configuration. The normal (forward) image correlation compares a deformed image with an undeformed image to extract the Lagrangian displacements (U, V) at selected grid points (X, Y) as shown in Fig. 3(a)

$$U(X, Y) = x - X, \quad V(X, Y) = y - Y. \tag{A2}$$

On the other hand, the *backward* image correlation compares the undeformed image with a deformed image to extract the Eulerian displacements (u, v) at selected grid points (x, y) as shown in Fig. 3(b)

$$u(x, y) = X - x, \quad v(x, y) = Y - y. \tag{A3}$$

The two types of the displacements of the same material point are simply related with each other via.

$$u(x, y) = -U(X, Y), \quad v(x, y), = -V(X, Y). \tag{A4}$$

One can also compute the Lagrangian displacement gradients based on the Eulerian displacement gradients obtained from the backward image correlation analysis, namely

$$\begin{aligned}
&\frac{\partial U(X, Y)}{\partial X} \\
&= \frac{-\dfrac{\partial u(x, y)}{\partial x}\left(1 + \dfrac{\partial v(x, y)}{\partial y}\right) + \dfrac{\partial u(x, y)}{\partial y}\dfrac{\partial v(x, y)}{\partial x}}{\left(1 + \dfrac{\partial u(x, y)}{\partial x}\right)\left(1 + \dfrac{\partial v(x, y)}{\partial y}\right) - \dfrac{\partial u(x, y)}{\partial y}\dfrac{\partial v(x, y)}{\partial x}}, \\
&\frac{\partial U(X, Y)}{\partial Y} \\
&= \frac{-\dfrac{\partial u(x, y)}{\partial y}}{\left(1 + \dfrac{\partial u(x, y)}{\partial x}\right)\left(1 + \dfrac{\partial v(x, y)}{\partial y}\right) - \dfrac{\partial u(x, y)}{\partial y}\dfrac{\partial v(x, y)}{\partial x}}, \\
&\frac{\partial V(X, Y)}{\partial X} \\
&= \frac{-\dfrac{\partial v(x, y)}{\partial x}}{\left(1 + \dfrac{\partial u(x, y)}{\partial x}\right)\left(1 + \dfrac{\partial v(x, y)}{\partial y}\right) - \dfrac{\partial u(x, y)}{\partial y}\dfrac{\partial v(x, y)}{\partial x}}, \\
&\frac{\partial V(X, Y)}{\partial Y} \\
&= \frac{-\left(1 + \dfrac{\partial u(x, y)}{\partial x}\right)\dfrac{\partial v(x, y)}{\partial y} + \dfrac{\partial u(x, y)}{\partial y}\dfrac{\partial v(x, y)}{\partial x}}{\left(1 + \dfrac{\partial u(x, y)}{\partial x}\right)\left(1 + \dfrac{\partial v(x, y)}{\partial y}\right) - \dfrac{\partial u(x, y)}{\partial y}\dfrac{\partial v(x, y)}{\partial x}},
\end{aligned} \tag{A5}$$

where an affine deformation of the continuum material point in 2D ensures that

$$\left(1 + \frac{\partial u(x, y)}{\partial x}\right)\left(1 + \frac{\partial v(x, y)}{\partial y}\right) - \frac{\partial u(x, y)}{\partial y}\frac{\partial v(x, y)}{\partial x} > 0. \tag{A6}$$